Modelling the hygro-mechanical creep behaviour of FRP reinforced timber elements

Conan O'Ceallaigh [a,*], Karol Sikora [b], Daniel McPolin [c], Annette M. Harte [a]

[a] College of Science and Engineering & Ryan Institute, National University of Ireland Galway, Ireland
[b] Faculty of Engineering and Information Sciences, University of Wollongong in Dubai, UAE
[c] School of Planning, Architecture and Civil Engineering, Queen's University Belfast, University Road, Belfast BT7 1NN, UK

HIGHLIGHTS

- A numerical model has been developed to predict the creep behaviour of timber elements.
- DFLUX and UMAT user subroutines describe the relative humidity and material behaviour.
- Recoverable and irrecoverable mechano-sorptive creep have been characterised.
- The creep behaviour of FRP reinforced beams has been accurately modelled.

ARTICLE INFO

ABSTRACT

A fully coupled moisture-displacement finite element model has been developed to predict the viscoelastic, mechano-sorptive and swelling/shrinkage behaviour of FRP reinforced timber elements when stressed under long-term load and simultaneously subjected to changes in relative humidity. A DFLUX subroutine, to describe the changes in relative humidity with time, and a UMAT subroutine, implemented to describe the viscoelastic, mechano-sorptive and swelling/shrinkage behaviour, are presented. Additionally, an irrecoverable mechano-sorptive component is presented. This additional irrecoverable component occurs when the timber moisture content increases to a moisture content above levels previously attained. The model is found to be in agreement with experimentally determined deflection and strain results on both unreinforced and FRP reinforced beams subjected to constant and variable climates.

© 2020 Elsevier Ltd. All rights reserved.

1. Introduction

FRP (Fibre Reinforced Polymer) materials are increasingly being used to strengthen and stiffen structural timber products [1–3]. This occurs in both new and existing timber construction and has been used to great effect when retrofitting structures. Changes in use of the building or, indeed, changes in building regulations often require a higher load capacity than that of the existing members. FRP reinforcement has been used successfully to achieve such additional capacity requirements [1–10] but the influence of FRP reinforcement on the long-term or creep behaviour of timber elements has received less attention. Creep in wood is often separated into two main categories, namely viscoelastic creep and mechanosorptive creep. Viscoelastic creep is defined as the deformation with time at constant stress under constant environmental conditions and it has been the subject of many investigations, which have examined the influence of stress [11,12], temperature [13], moisture content [14] and flexural reinforcement on the long-term viscoelastic behaviour of timber elements [15–18]. Mechano-sorptive creep behaviour is defined as a deformation due to the interaction between stress and moisture content change in timber elements. Under variable environmental conditions, the mechano-sorptive effect can greatly accelerate the creep deflection of a timber element and ultimately lead to failure. The prediction of

---

* Corresponding author.

E-mail addresses: conan.oceallaigh@nuigalway.ie (C. O'Ceallaigh), karolsikora@uowdubai.ac.ae (K. Sikora), d.mcpolin@qub.ac.uk (D. McPolin), annette.harte@nuigalway.ie (A.M. Harte).

long-term effects and the influence of reinforcement on these timber beams are of crucial importance to structural engineers when designing timber structures.

Rheology is the study of the flow of matter and rheological models can be used to describe time-dependent viscoelastic behaviour in timber elements. The basic elements of these models are known as spring and dashpot elements. When combining springs and dashpots in series and/or parallel, rheological or viscoelastic models can be created [19]. In practical applications, generalised models are required to accurately model viscoelastic material behaviour. Generalised models combine a number of springs and dashpot elements, which increases the number of parameters and gives a better representation of the behaviour of the material being studied [11,20]. When modelling the long-term behaviour of timber elements, the surrounding environment must be considered given its significant effect on the material properties and creep behaviour. Many researchers have attempted to predict the effects of variable humidity and associated moisture fluctuations on timber elements and to model mechano-sorptive behaviour [21–25]. Leicester [21] and Ranta-Maunus [22,26] developed some of the first models in an attempt to quantify the mechano-sorptive effect in timber. Leicester [21] produced a uniaxial model consisting of an elastic component and an irrecoverable mechano-sorptive component. The predicted results were compared with experimental data from a small sample of Eucalyptus during two weeks of drying. This rheological model was found to predict 85% of the total deformation recorded during testing. In a later study, Fridley et al. [27] developed a sophisticated model based on the Burger model, which included mechano-sorptive creep effects, but also included moisture and temperature dependent variations in stiffness. This adaption provided good agreement between modelled and experimental strain data. Mohager & Toratti [28] presented a mechano-sorptive model incorporating different tensile and compressive compliance functions and a model including partially irrecoverable compressive strains was proposed. Mårtensson [25] developed another model that decomposed the total strain into elastic, viscoelastic, shrinkage/swelling, and mechano-sorptive creep strain components. Lu & Leicester [29] presented a mechano-sorptive model coupled with a simple approximate solution for moisture variation within a specimen based on Fick's law of diffusion and sinusoidal fluctuations in ambient moisture boundary conditions. Hanhijärvi & Mackenzie-Helnwein [30] presented an orthotropic material model based on a one-dimensional model presented by Hanhijärvi [31] incorporating elastic, viscoelastic, mechano-sorptive and swelling/shrinkage strains. The mechano-sorptive strain component is altered to incorporate permanent deformations by introducing a hardening type plasticity element. This was found to accurately describe the deformations associated with high temperature drying in timber elements. Fortino et al. [32] presented a three-dimensional model for analysing timber structures under variable humidity and stress conditions. The viscoelastic/mechano-sorptive constitutive model is implemented in the user subroutine UMAT of the finite element modelling code Abaqus. They used Fick's law to describe moisture flow within the timber element. This Fickian behaviour was implemented into the Abaqus user-defined DFLUX subroutine. The model was successfully validated against experimental results by Leivo [33], Toratti & Svensson [34], Svensson & Toratti [35] and Jönsson [36]. Such advanced models have been used to examine a range of different challenges facing the timber industry and have contributed to increased knowledge and safer structures. Fragiacomo et al. [37] utilised an advanced numerical model to compute the moisture distribution and corresponding stresses or moisture-induced stresses in timber elements subjected to different climates which demonstrated that northern European climates can be more severe than southern climates. Massaro et al. [38,39] applied such

models to examine timber elements subjected to compression perpendicular to the grain. This has been further advanced in recent years to included multi-Fickian transport theory which examines the influence of changes in both water vapour and bound water on timber structures [24,40]. Huč et al. [40] developed a model to successfully predict strains in timber elements subjected to sustained compressive loading. Fortino et al. [24] recently presented an advanced study incorporating a multi-Fickian hygro-thermal model capable of simulating severe changes in relative humidity and temperature. The study presented the associated moisture fluctuations and moisture-induced stresses on a bridge in the north of Sweden which is subjected to harsh climatic conditions over a 10-year analysis.

While many models have been developed to examine the effect of FRP reinforcement on the mechanical properties of timber elements, the majority of these models focus on the short-term performance and are not concerned with viscoelastic creep, mechano-sorptive, temperature and moisture effects. A two-dimensional model was developed by Tingley [41] to examine the stress-strain relationship of FRP reinforced glued laminated beams. This model did not include plasticity, creep, temperature or moisture effects and solely focused on the short-term elastic response. Serrano [42] modelled timber connections with bonded-in rods. The timber was modelled as a linear elastic orthotropic material and it was found that the stress concentrations were greatly influenced by the reinforcement stiffness and thickness. In another study, Alam [43] implemented anisotropic plasticity in a three-dimensional model to predict flexural properties of LVL beams reinforced with bonded-in FRP reinforcement. This model compared well with experimental findings. Raftery & Harte [44] also employed anisotropic plasticity theory in a model to predict the behaviour of unreinforced and glass fibre reinforced glued laminated beams. The model results agreed strongly with experimental results and a parametric study showed that as the reinforcement percentage is increased, the stiffness and ultimate moment capacity are enhanced.

A relatively low number of studies have attempted to predict the long-term performance of FRP reinforced beams under constant or variable climate conditions and these have been limited to the uniaxial case. In a study by Plevris & Triantafillou [15], an analytical model is employed to predict the creep behaviour of CFRP reinforced timber beams. The model, based on a Burger element, was developed to account for moisture effects. The experimental and analytical data showed good agreement in a constant climate; however, only limited experimental data was available. In Davids et al. [45], a uniaxial model was developed to model the creep behaviour of GFRP reinforced timber beams in a variable climate. The model, combining viscoelastic and mechano-sorptive creep strain parameters, was fitted using unreinforced specimen test results and then shown to accurately predict the relative creep deflection of glass FRP reinforced beams in a variable climate.

Numerical modelling can be an important tool when modelling complex materials such as timber. It has also been shown to adequately model various reinforcement materials in various configurations. These advances in numerical modelling have increased the reliability of results and as a result can aid future product development. The recent advances in modelling unreinforced timber by Hanhijärvi & Mackenzie-Helnwein [30] and Fortino et al. [24,32,46] are yet to be specialised for reinforced timber elements under changing relative humidity conditions.

1.1. Objectives of the current study

The objective of the current numerical study is to develop a model to predict the influence of flexural reinforcement on the long-term creep behaviour of timber beams in constant and vari-

able climates. The numerical model presented is developed using Abaqus finite element analysis software [47]. As mechano-sorptive creep is not explicitly available in Abaqus, a user-defined UMAT subroutine is required to define mechano-sorptive behaviour during loading and simultaneous moisture diffusion within timber. The moisture content distribution within the timber and associated strains are determined in a fully coupled time-dependent hygro-mechanical analysis. A DFLUX subroutine is utilised to describe the interaction between the surrounding environment and the surface of the timber in the model. Such models have been shown to successfully replicate deflection and stress development in fluctuating environments by Mirianon et al. [48] and Fortino et al. [32]. In this study, the formulation of the UMAT subroutine follows the approach implemented by Santaoja et al. [49], Mårtensson [50], Mirianon et al. [48] and Fortino et al. [32]; however, a significant alteration was made to the irrecoverable mechano-sorptive creep matrix to include irrecoverable deformations in the longitudinal direction when stressed under loaded conditions and subject to moisture contents not previously attained. The coupled hygro-mechanical model is compared to the experimental creep deflection and strain tests results on unreinforced and FRP reinforced elements subjected to four-point bending tests presented by O'Ceallaigh et al. [17,51–54].

2. Materials

In this study, timber is modelled as an orthotropic elastic material in Abaqus. The Sitka spruce material tested experimentally by O'Ceallaigh et al. [17,51–53] was graded to strength class C16. The standard EN 338 [55] provides a mean value of 8000 MPa for the elastic modulus of C16 timber in the longitudinal direction; however, the experimentally determined elastic modulus in the longitudinal direction of 9222 N/mm^2, determined from short-term static bending tests, is used. The elastic moduli in the radial and tangential directions were not measured experimentally; however, Bodig & Jayne [56] expressed a general relationship between the elastic modulus, E and shear modulus, G in the three material directions. These ratios are reproduced in Eqs. (1)–(3).

$$E_L : E_R : E_T \approx 20 : 1.6 : 1 \tag{1}$$

$$G_{LR} : G_{LT} : G_{RT} \approx 10 : 9.4 : 1 \tag{2}$$

$$E_L : G_{LR} \approx 14 : 1 \tag{3}$$

These ratios are widely accepted for modelling the orthotropic properties of timber. However, it is noted that these ratios are not without their inaccuracies. The size of a timber element and the location it was cut from a log are factors in the accuracy of the assumption. More information on the timber material properties is given in Table 1. Additionally, these material properties are also dependent on the density, temperature and moisture content of the timber. Eqs. (4) and (5) are implemented to adjust the elastic and shear modulus properties when the environmental conditions are different from the reference conditions [49].

$$E_i = E_{i,ref}\left\{1 + \alpha_1\left(\rho - \rho_{ref}\right) + \alpha_2\left(T - T_{ref}\right) + \alpha_3\left(u - u_{ref}\right)\right\} \tag{4}$$

$$G_{ij} = G_{ij,ref}\left\{1 + \alpha_1\left(\rho - \rho_{ref}\right) + \alpha_2\left(T - T_{ref}\right) + \alpha_3\left(u - u_{ref}\right)\right\} \tag{5}$$

$E_{i,ref}$ and $G_{ij,ref}$ are the reference elastic modulus and shear modulus, respectively, which correspond to the reference density (ρ_{ref} - kg/m^3), temperature (T_{ref} - °C) and moisture content (u_{ref} - %). ρ, T and u refer to the current density, temperature and moisture con-

tent, respectively, at any given time step and α_1 = 0.0003, α_2 = −0.007 and α_3 = −2.6 are material constants provided by Santaoja et al. [49] and Mirianon et al. [48].

The FRP rod reinforcement and epoxy adhesive in reinforced members are modelled as linear elastic materials. Experimental tests have shown that the reinforcement is negligibly affected by swelling and shrinkage or creep and have not been considered in the study [51]. The material properties implemented in the model are presented in Table 2.

3. Finite element formulation

In this section, the constitutive models used to simulate the moisture diffusion and deformation of timber beams in both constant and variable climates are described. The formulation presented for deformation follows the approach implemented by Santaoja et al. [49], Mårtensson [50], Mirianon et al. [48] and Fortino et al. [32] but is adapted to represent Irish-grown Sitka spruce using experimental data. In the fully coupled 3-dimensional finite element model, a UMAT subroutine to determine the total strain experienced in timber elements when subjected to mechanical stress and simultaneous moisture content changes with time is implemented. This simulated total strain is subdivided into five separate strain components. These strain components are solved for in an incremental analysis with time. The total strain ε_{Total}, is given in Eq. (6).

$$\varepsilon_{Total} = \varepsilon_e + \sum_{i=1}^{k} \varepsilon_{ve} + \varepsilon_{ms} + \varepsilon_{ms,irr} + \varepsilon_s \tag{6}$$

where ε_e = Elastic strain component, ε_{ve} = Viscoelastic strain component, ε_{ms} = Mechano-sorptive strain component, $\varepsilon_{ms,irr}$ = Irrecoverable mechano-sorptive strain component and ε_s = Swelling/shrinkage strain component. The k term denotes the number of viscoelastic Kelvin elements used in the formulation of the viscoelastic creep component. The modelling of diffusion moisture through the cross section within a coupled moisture-displacement analysis is presented as is the transfer of moisture content from the surrounding environment which is defined through the use of a DFLUX subroutine.

3.1. Elastic strain component

The elastic component (ε_e) follows the generalised Hooke's law as seen in Eq. (7) where σ is the stress and C_e is the elastic compliance matrix of an orthotropic material. In 3-dimensional matrix form, this equation defines the orthogonal elastic stress–strain behaviour of timber (Eq. (8)).

$$\varepsilon_e = C_e \sigma \tag{7}$$

$$C_e = \begin{bmatrix} \frac{1}{E_R} & -\frac{v_{TL}}{E_T} & -\frac{v_{LR}}{E_L} & 0 & 0 & 0 \\ -\frac{v_{RT}}{E_R} & \frac{1}{E_T} & -\frac{v_{LT}}{E_L} & 0 & 0 & 0 \\ -\frac{v_{RL}}{E_R} & -\frac{v_{TL}}{E_T} & \frac{1}{E_L} & 0 & 0 & 0 \\ 0 & 0 & 0 & \frac{1}{G_{RT}} & 0 & 0 \\ 0 & 0 & 0 & 0 & \frac{1}{G_{RL}} & 0 \\ 0 & 0 & 0 & 0 & 0 & \frac{1}{G_{TL}} \end{bmatrix} \tag{8}$$

The elastic compliance matrix is symmetric, and the Poisson's ratios are related according to Eq. (9).

$$v_{RL} = \frac{E_R}{E_R}v_{LR} \qquad v_{TL} = \frac{E_T}{E_L}v_{LT} \qquad v_{TR} = \frac{E_T}{E_R}v_{RT} \tag{9}$$

Table 1
Timber material data.

Notation	Description		Property Value	Unit	Source
E_R	Radial elastic modulus		663	MPa	Eqs. (1)-(3) [56]
E_T	Tangential elastic modulus		415	MPa	
E_L	Longitudinal elastic modulus		9222	MPa	Experimental test results [51]
v_{RT}	Poisson's ratio radial-tangential		0.558	-	[32,48,49]
v_{RL}	Poisson's ratio radial-longitudinal		0.038	-	
v_{TL}	Poisson's ratio tangential-longitudinal		0.015	-	
G_{RT}	Shear modulus radial-tangential		66	MPa	Eqs. (1)-(3) [56]
G_{RL}	Shear modulus radial-longitudinal		659	MPa	
G_{TL}	Shear modulus tangential-longitudinal		619	MPa	
α_1	Alpha density		0.0003	m³/kg	[32,48,49]
α_2	Alpha temp		-0.007	1/°C	
α_3	Alpha moisture content		-2.6	-	
ρ_{ref}	Reference density		400	kg/m³	O'Ceallaigh et al. [61]
T_{ref}	Reference temperature		20	°C	
u_{ref}	Reference moisture Content		0.12	-	
u_{FSP}	Fibre saturation Point		0.28	-	
α_R	Radial moisture expansion coefficient		0.1371	-	O'Ceallaigh et al. [61]
α_T	Tangential moisture expansion coefficient		0.2525	-	
α_L	Longitudinal moisture expansion coefficient		0.0122	-	
τ_1	Characteristic Time	Kelvin Element No. 1	20	hr	Fortino et al. [32], Mirianon et al. [48] and matched to experimental test results [51]
$J_{ve,1}$	Viscoelastic compliance ratio		0.06	-	
τ_2	Characteristic Time	No. 2	200	hr	
$J_{ve,2}$	Viscoelastic compliance ratio		0.05	-	
τ_3	Characteristic Time	No. 3	2000	hr	
$J_{ve,3}$	Viscoelastic compliance ratio		0.055	-	
τ_4	Characteristic Time	No. 4	20000	hr	
$J_{ve,4}$	Viscoelastic compliance ratio		0.285	–	
m_L	Longitudinal irrecoverable mechano-sorptive parameter		0.70	1/GPa	Experimental test results [51]
m_V	Radial/tangential irrecoverable mechano-sorptive parameter		0.13	1/MPa	
$m_{ms,R}$	Mechano-sorptive creep matrix parameters		0.01	1/MPa	Santaoja et al. [49], Ormarsson et al. [60] and matched to experimental test results [51]
$m_{ms,T}$			0.02	1/MPa	
$m_{ms,L}$			0.40	1/GPa	
$v_{ms,RT}$			0.50	–	
$v_{ms,RL}$			0.04	–	
$v_{ms,TL}$			0.02	–	
$m_{ms,RT}$			0.10	1/MPa	
$m_{ms,RL}$			8.00	1/GPa	
$m_{ms,TL}$			8.00	1/GPa	
D_L	Longitudinal diffusion coefficient at u_{ref}		3.3×10^{-10}	m²/s	Experimental test results [51], O'Ceallaigh et al. [61]
D_R	Radial diffusion coefficient at u_{ref}		1.6×10^{-11}	m²/s	
D_T	Tangential diffusion coefficient at u_{ref}		1.6×10^{-11}	m²/s	

Table 2
BFRP and epoxy adhesive material data.

Notation	Description	Property Value	Unit	Source
E_{BFRP}	BFRP rod reinforcement elastic modulus	50,772	MPa	Experimental test results [51]
v_{BFRP}	Poisson's ratio BFRP rod reinforcement	0.3	–	Zachary & Kavan [65]
E_{EPOXY}	Epoxy adhesive elastic modulus	3700	MPa	Manufacturers data sheet [66]
v_{EPOXY}	Poisson's ratio Epoxy adhesive	0.29	–	Konnerth et al. [67]

The subscripts *L*, *R* and *T* refer, respectively, to the directions of assumed elastic symmetry, longitudinal, radial and tangential directions. *E* and *G* represent the elastic modulus and shear modulus, respectively. Bodig & Jayne [56] expressed a general relationship between the moduli *E* (elastic) and *G* (shear) in the three orientations as presented in Eqs. (1)–(3). These material properties of timber are dependent on the moisture content, temperature and density of the timber. Eqs. (4) and (5) are implemented to adjust the elastic and shear modulus properties when the environmental conditions are different from the reference conditions [49].

3.2. Viscoelastic strain component

The additional deformation with time in timber elements loaded under constant stress is known as viscoelastic creep. In this study, the viscoelastic strain component (ε_{ve}) is an extension of the one-dimensional model presented by Toratti [12] consisting of a sum of Kelvin type elements as illustrated in Fig. 1.

The stress–strain relationship describing the time-dependent behaviour of a Kelvin element is described in Eq. (10) [19,30,32].

$$\dot{\varepsilon}_{ve,i} + \frac{1}{\tau_i}\varepsilon_{ve,i} = \frac{1}{\tau_i}C_{ve,i}^{-1}\sigma \tag{10}$$

where $\dot{\varepsilon}_{ve,i}$ = the viscoelastic strain rate = $\frac{\partial}{\partial t}\varepsilon_{ve,i}$, $C_{ve,i}$ = the viscoelastic compliance matrix of the ith Kelvin element, σ = the total stress in the ith Kelvin element and τ_i = the retardation or characteristic time of the ith Kelvin element. It has been shown by Hanhijarvi & Mackenzie-Helnwein [30] and Fortino et al. [32] that for stress-driven problems, the solution to the rate equation (Eq. (10)) can be written as,

$$\varepsilon_{ve,i,n+1} = \varepsilon_{ve,i,n}\exp\left(\frac{-\Delta t}{\tau_i}\right) + \int_{t_n}^{t_{n+1}}\frac{C_{ve,i}^{-1}\sigma}{\tau_i}\exp\left(-\frac{(t_{n+1}-t_n)}{\tau_i}\right)dt \tag{11}$$

where $\varepsilon_{ve,i,}$ = viscoelastic strain of the ith Kelvin element and Δt = the time increment ($t_{n+1} - t_n$). By integrating this expression for viscoelastic strain (Eq. (11)) over time for the ith Kelvin element, the following increment of elemental viscoelastic strain is obtained [48,57].

$$\Delta\varepsilon_{ve,i,n+1} = C_{ve,i}T_{i,n+1}\left(\frac{\Delta t}{\tau_i}\right)\Delta\sigma_{n+1} - (\varepsilon_{ve,i,n} - C_{ve,i}\sigma_n)\left(1 - \exp\left(-\frac{\Delta t}{\tau_i}\right)\right) \tag{12}$$

where:

$$T_{i,n+1}\left(\frac{\Delta t}{\tau_i}\right) = 1 - \frac{\tau_i}{\Delta t}\left(1 - \exp\left(-\frac{\Delta t}{\tau_i}\right)\right) \tag{13}$$

$$C_{ve,i} = J_{ve,i}C_e \tag{14}$$

where $J_{ve,i}$ represents the dimensionless viscoelastic compliance ratio of the ith Kelvin element.

3.3. Total mechano-sorptive strain component

The total mechano-sorptive strain component ($\varepsilon_{ms,Total}$) consists of two individual components as seen in Eq. (15). Both of these components occur under coupled stress and moisture content change associated with relative humidity variations in the surrounding environment.

$$\varepsilon_{ms,Total} = \varepsilon_{ms,irr} + \varepsilon_{ms} \tag{15}$$

where $\varepsilon_{ms,irr}$ = irrecoverable mechano-sorptive strain component and ε_{ms} = mechano-sorptive strain component.

The increment of the irrecoverable component of mechano-sorptive strain is calculated using Eq. (16) [32,35]. It is independent of stress rate and is a permanent deformation proportional to the current stress state and change in moisture content [58].

$$\Delta\varepsilon_{ms,irr,n+1} = C_{ms,irr}\,\sigma_n|\Delta U| \tag{16}$$

where $\Delta\varepsilon_{ms,irr}$ = irrecoverable mechano-sorptive strain increment, $C_{ms,irr}$ = irrecoverable mechano-sorptive compliance matrix (Eq. (17)), σ_n = stress state at time $t = t_n$ and ΔU = increase in moisture content above levels attained during previous moisture cycles. The irrecoverable mechano-sorptive matrix previously presented by Fortino et al. [32] accounts for irrecoverable deformations in the radial and tangential directions only. As a novelty of this research project, it was shown experimentally that the development of irrecoverable mechano-sorptive creep strains are also observed in the longitudinal direction. As a result, Fortino's formulation has been modified to account for irrecoverable strains (m_L) in the longitudinal direction as seen in Eq. (17). The value of the irrecoverable coefficient in the radial/tangential direction, m_v presented by Fortino et al. [32] and the longitudinal direction, m_L have been determined through careful calibration against experimental results on unreinforced beams.

$$C_{ms,irr} = \begin{bmatrix} m_v\frac{E_T}{E_R} & -m_v\frac{E_T}{E_R}V_{RT} & -m_v\frac{E_T}{E_R}V_{RL} & 0 & 0 & 0 \\ -m_v\frac{E_T}{E_R}V_{RT} & m_v & -m_v\frac{E_T}{E_R}V_{TL} & 0 & 0 & 0 \\ -m_v\frac{E_T}{E_R}V_{RL} & -m_v\frac{E_T}{E_R}V_{TL} & m_L & 0 & 0 & 0 \\ 0 & 0 & 0 & m_v\frac{E_T}{G_{RT}} & 0 & 0 \\ 0 & 0 & 0 & 0 & m_v\frac{E_T}{G_{RL}} & 0 \\ 0 & 0 & 0 & 0 & 0 & m_v\frac{E_T}{G_{TL}} \end{bmatrix} \tag{17}$$

where m_L = Longitudinal irrecoverable strain coefficient and m_v = Radial/tangential Irrecoverable strain coefficient.

When describing the recoverable mechano-sorptive strain associated with repeating cycles of relative humidity, the schemes previously implemented by Santaoja et al. [49] Mårtensson [50] and Ormarsson [59] have been implemented. The solution is found using the absolute value of moisture content, which is assumed to be constant over the time increment.

$$\Delta\varepsilon_{ms,n+1} = C_{ms}\sigma_n|\Delta u| \tag{18}$$

where: $\Delta\varepsilon_{ms}$ = mechano-sorptive strain increment, C_{ms} = mechano-sorptive compliance matrix (Eq. (19)) σ_n = stress state at time $t = t_n$ and $|\Delta u|$ = the moisture increment $|u_{n+1} - u_n|$.

The elemental mechano-sorptive compliance matrix assumes the form given in Eq. (19) [49,50,59].

$$C_{ms} = \begin{bmatrix} m_{ms,R} & -m_{ms,T}v_{ms,RT} & -m_{ms,L}v_{ms,LR} & 0 & 0 & 0 \\ -m_{ms,R}v_{ms,RL} & m_{ms,T} & -m_{ms,L}v_{ms,LT} & 0 & 0 & 0 \\ -m_{ms,R}v_{ms,RL} & -m_{ms,T}v_{ms,TL} & m_{ms,L} & 0 & 0 & 0 \\ 0 & 0 & 0 & m_{ms,RT} & 0 & 0 \\ 0 & 0 & 0 & 0 & m_{ms,RL} & 0 \\ 0 & 0 & 0 & 0 & 0 & m_{ms,TL} \end{bmatrix} \tag{19}$$

The coefficients of the matrix (C_{ms}) are based on the mechano-sorptive compliance coefficients ($m_{ms,i}$) in the respective material directions and, using the ratios $v_{ms,i}$, to describe the coupling of
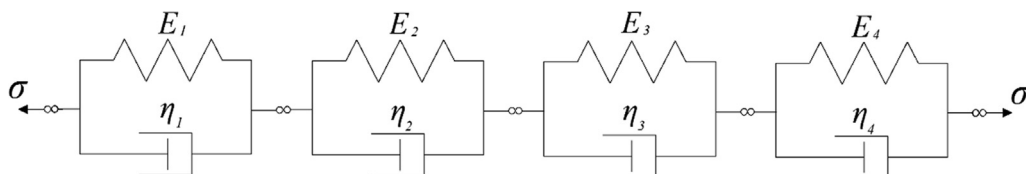
Fig. 1. A system of four Kelvin elements connected in series: Each Kelvin element comprises a spring (E) and viscous dashpot (η) in parallel.

the mechano-sorptive strain between the different directions. The values used have been based on previous research by Santaoja et al. [49] and Ormarsson et al. [60] and finally matched to experimental test results.

3.4. Swelling/shrinkage strain component

Swelling/shrinkage strains (ε_s) occur within the timber during moisture content change. This change in strain depends on the material direction and magnitude of the change in moisture content. The increment in ε_s due to a moisture content change, Δu, is described by Eq. (20).

$$\Delta\varepsilon_s = \alpha_u\Delta u \tag{20}$$

where the moisture swelling/shrinkage vector α_u is described by Eq. (21).

$$\alpha_u = \begin{bmatrix} \alpha_R \\ \alpha_T \\ \alpha_L \\ 0 \\ 0 \\ 0 \end{bmatrix} \tag{21}$$

The components of the swelling/shrinkage vector (α_u) used in the study were determined experimentally [61]. It has been found that different loading conditions (tension, compression or bending) result in different longitudinal swelling/shrinkage behaviour of timber. Wood tends to swell/shrink less when in tension and swell/shrink more in compression [62]. Toratti [23] implements an adapted formula (Eq. (22)) to account for variations in longitudinal strain when in a state of tension and compression as is the case in bending.

$$\Delta\varepsilon_{s,L} = (\alpha_L - \beta\varepsilon_{mech,L})\Delta u \tag{22}$$

where β = Material constant = 1.3 (Mirianon et al. [48]) and $\varepsilon_{mech,L}$ = longitudinal component of the mechanical strain vector. This is applied to the longitudinal direction in the developed model. A similar approach has been used in Mohager & Toratti [28], Hanhijarvi [58] and Davids et al. [63].

3.5. Diffusion modelling

Fick's law, which describes the moisture diffusion process, is analogous to Fourier's law of heat transfer. Using this analogy, the governing equations allow diffusion coefficients and moisture content to replace thermal conductivity and temperature. This allows coupled temperature-displacement elements in Abaqus to be exploited in a hygro-mechanical model to simulate coupled moisture diffusion and mechanical behaviour. The environmental load or relative humidity load is implemented in Abaqus through a DFLUX user subroutine in order to apply a defined time-dependent relative humidity boundary condition. The transport of moisture across the surface of the timber is proportional to the difference between the equilibrium moisture content of the surface of the timber and the equilibrium moisture content of the timber corresponding to the relative humidity of the surrounding environment. In the DFLUX subroutine, the rate of moisture transport between the surface of the timber and the surrounding environment is governed by Eq. (23).

$$q_n = \rho S_u(u_{eq} - u_{surf}) \tag{23}$$

where q_n = rate of moisture flow, ρ = density at 0% moisture content, u_{eq} = equilibrium moisture content of timber corresponding to the relative humidity of the surrounding environment and u_{surf} =

moisture content of the timber surface. The surface emissivity S_u defines the rate of moisture content exchange across the boundary and is a function of the environment, the characteristics of the timber surface and is also dependent on the velocity of the circulating air [58]. The value used in this model of $3.2 \times 10^{-8}\ e^{4.0u}$ m/s was previously reported by Hanhijärvi [58] where u is moisture content. More information related to the diffusion coefficients and the influence of relative humidity on the equilibrium moisture content (u_{eq}) of the timber used in this study is provided by O'Ceallaigh et al. [61], which focuses on moisture-induced strains in fast-grown timber. In the current study, the environmental load is applied to the exposed surfaces of the beam. In line with the experimental tests [17,51–54], the exposed surfaces include both sides of the glued laminated beam and the top surface only. The BFRP reinforcement in the tension zone of the reinforced beams impedes the movement of moisture through the bottom and end grain surfaces. As a result, the bottom and end grain surfaces were sealed for both unreinforced and reinforced beams to ensure all beams are subject to the same exposure conditions.

4. Hygro-mechanical creep model

4.1. Model geometry

The geometry of unreinforced and FRP reinforced beams, which are subjected to a creep test in four-point bending, [17,51,53] is modelled using Abaqus finite element software. As seen in Fig. 2, the 98 × 125 mm² unreinforced and reinforced beams comprise four laminations. Each of the four laminations is assigned material properties in a local cylindrically orientated coordinate system. The glue-line between laminations was not modelled in this study due to the good performance of the glue-line under variable climates and its limited influence on the moisture diffusion behaviour through the cross-section of the timber as shown by Raftery et al. [64] and O'Ceallaigh et al. [61], respectively. The FRP reinforced beam model is similar to that of the unreinforced beam; however, in the bottom tensile lamination, two routed grooves are created to accommodate the two 12 mm diameter basalt fibre reinforced polymer (BFRP) rods and the 2 mm structural epoxy adhesive. Both models use 8-noded coupled thermal-displacement C3D8T elements. As seen in Fig. 3, symmetry is utilised allowing only half of the 2300 mm long beam to be modelled to reduce the computational time. The respective mesh sizes for the unreinforced and reinforced beam models were determined from mesh sensitivity studies to provide accurate results in a reasonable time frame. The beam is simply supported on 80 mm × 100 mm plates which are free to rotate about their central axis. These plates are modelled using 2-dimensional shell S3 elements. Hard contact is defined between the surface of the beam and the steel plate with a tangential friction coefficient of 0.4. Similar plates are used to apply the dead load in tests. These are also modelled using S3 shell elements and the load is applied as a uniform pressure over the plate area.

Regarding the numerical models, a load of 5749 N was applied to the unreinforced beams and a load of 6241 N was applied to the reinforced beams to induce a common maximum compressive bending stress of 8 MPa in each beam as was done experimentally by O'Ceallaigh et al. [17,51].

4.2. Material data

This section presents the material data for the timber, epoxy adhesive and BFRP implemented in the numerical models. The timber material data is summarised in Table 1. The BFRP rod reinforce-
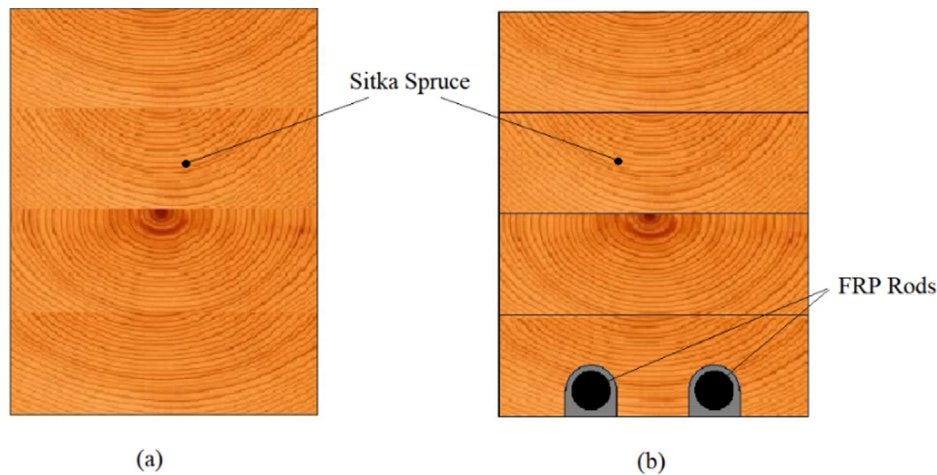
Fig. 2. Beam cross-sections: (a) Unreinforced beam, (b) Reinforced beam.
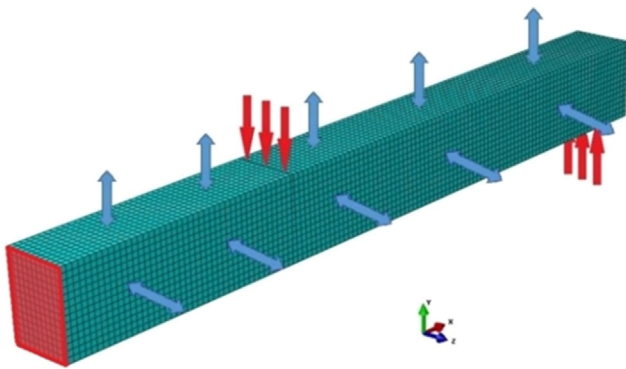
Fig. 3. Finite element coupled hygro-mechanical creep model of the unreinforced glued laminated beam: The plane of symmetry is highlighted in red at the mid-span of the beam. The red arrows represent the load point and support point on the top and bottom surface, respectively, and the blue arrows represent the relative humidity load shown on the exposed surfaces (Note: Bottom and end grain surfaces were sealed on unreinforced and reinforced beams). (For interpretation of the references to colour in this figure legend, the reader is referred to the web version of this article.)

ment and epoxy adhesive material data implemented into the mechanical model are presented in Table 2.

4.3. Climate conditions

The numerical model is compared to experimental creep results on beams in both a constant and variable climate [17,51–53]. The constant climate remains at a relative humidity of 65% and a temperature of 20°C for the duration of the test. The variable climate condition induces mechano-sorptive creep and swelling/shrinkage strains due to hygro-expansion. This occurs due to the change in the relative humidity and subsequent change in the moisture content of the beams. Testing commenced at a relative humidity of 65% and at a temperature of 20 °C for a period of three weeks, after which, the relative humidity in the variable climate chamber was changed to 90%. After three weeks, the variable relative humidity cycle commenced with an increase in the relative humidity to 90% for four weeks followed by four weeks at a relative humidity of 65%.

4.4. Unreinforced beam model results

In this section, the results of the long-term numerical simulation of the unreinforced beam model in constant and variable cli-

mates are compared to the mean experimental result presented by O'Ceallaigh [51]. The experimental groups presented comprised of nine beams each [51]. The predicted total vertical deflection is compared to the experimental results in Fig. 5. The predicted initial elastic deflection of 6.09 mm compares well with the mean measured values of 6.27 mm (Group UC) and 5.95 mm (Group UV). Over the 75-week test period, it can be seen that the total mean long-term vertical deflection of Group UC beams is simulated accurately with a final predicted deflection of 8.08 mm compared to a measured mean value of 8.03 mm. This is to be expected as the viscoelastic compliance coefficients defined in Table 1 and used in this unreinforced model have been calibrated against the mean experimental deflection data from the unreinforced beams. It was important to accurately define the viscoelastic compliance coefficients of the unreinforced beams prior to simulating creep in reinforced beams.

In the variable climate condition, during the first three weeks, the relative humidity remains constant and, as a result, this period is solely associated with elastic and viscoelastic creep. Consequently, the numerical result for Group UV produced the same elastic deformation and viscoelastic creep as the constant climate model during this three-week period. After the first three weeks, the relative humidity increased resulting in an increase in moisture content which in turn leads to a significant increase in deflection due to irrecoverable mechano-sorptive creep (Fig. 4.) Significant increases in deflection and strain in the first relative humidity cycle have been previously reported due to changes in moisture content higher than that previously attained under a loaded condition [68]. After week 7 the relative humidity reverts to 65% from 90% and the relative humidity continues this 8 week cycle for 75 weeks. The numerical deflection result after 75 weeks of 12.48 mm agreed well with the mean experimentally determined Group UV deflection of 12.09 mm demonstrating the effectiveness of the numerical model in the prediction of the creep deflection of timber elements in both constant and variable climates.

The mean total longitudinal strain measured on the tension and compression faces of the unreinforced Group UC and Group UV beams are presented and compared to the numerical model predictions in Fig. 5. The results of the numerical model agree well with the mean experimental strain results measured on the tension and compression faces. In a constant climate, the model accurately predicts the initial elastic strain and viscoelastic creep strain on the tension and compression faces. After 75 weeks, on the tension face, the experimental result of 853 µε compared well to the numerical result of 904 µε and on the compression face the experimental
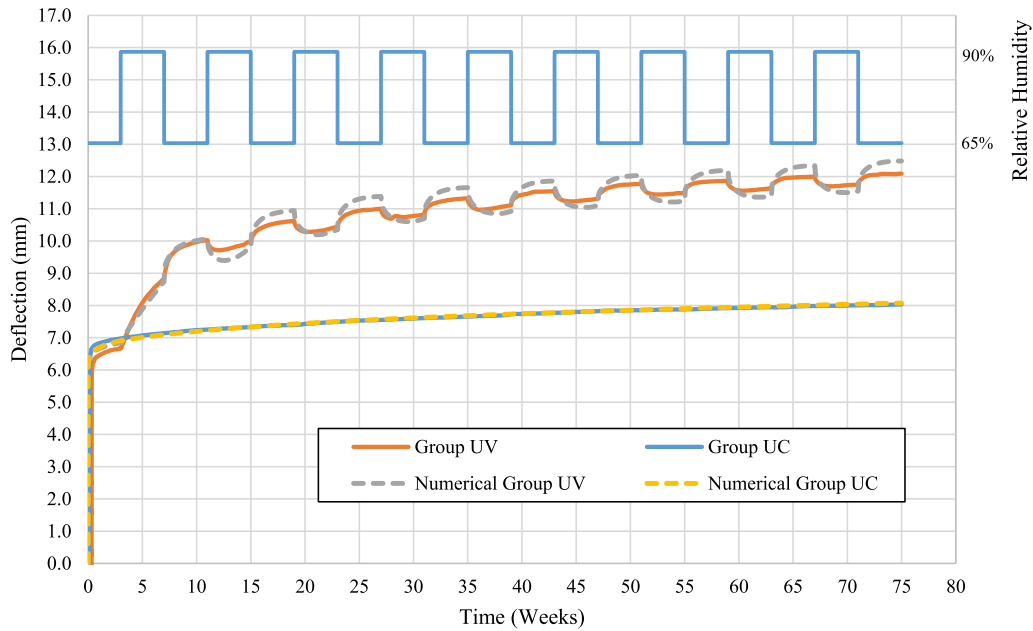
Fig. 4. Mean deflection result of Group UC (Constant climate) and Group UV (Variable climate) vs the numerical result.
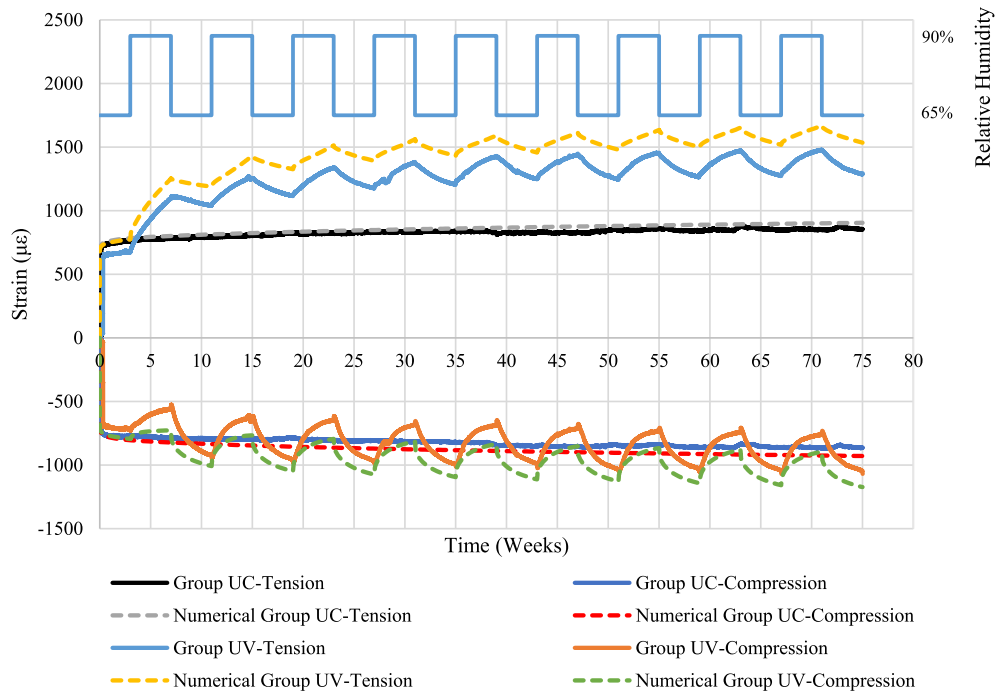
Fig. 5. Mean unreinforced Group UC (Constant climate) and Group UV (Variable climate) experimental vs numerical longitudinal strain results.

result of -864 µε compared well to the numerical result of -929 µε. The total mean strains measured on the tension and compression faces of Group UV in a variable climate have also been measured and are compared to the numerical model results in Fig. 5. The mean initial elastic strain has been slightly over estimated on both the tension and compression faces of the Group UV beams. After the initial elastic component, the model appears to adequately predict the total strain on the tension and compression face of the Group UV beams in a variable climate. The large increase in longitudinal strain during the first moisture content change attributed to the irrecoverable mechano-sorptive component has been simulated.

The fluctuation in strain with repeated cycles has been successfully simulated with the numerical model. On the tension face, the change in strain with each relative humidity cycle is more gradual than that experienced on the compression face. This is a result of the different exposure conditions of the tension and compression faces. The bottom (tension) face is sealed from the surrounding environment resulting in a reduced rate of moisture content change and more steadily increasing and decreasing rate of strain development in the tension face. After 75 weeks, the experimental tensile strain of 1294 µε compared reasonably well to the numerical result of 1535 µε and the experimental compressive strain of -1069 µε compared well to the numerical result of -1174 µε. It

can be seen that the results of the numerical model slightly over predict the mean experimental strain results measured on the tension and compression faces of the unreinforced beams. This over prediction is partially due to initial differences in the elastic strain.

4.5. Reinforced beam model results

The simulated numerical deflection for the reinforced beam model in constant and variable climates is compared to the mean experimental result of Group RC and Group RV, respectively in Fig. 6. Group RC and Group RV comprised nine beams each [51]. The addition of the BFRP reinforcement has resulted in a reduced initial elastic deflection and reduced long-term deflection after 75 weeks when compared to the unreinforced Groups UC and UV. The reduction in initial elastic deflection has been accurately predicted using the model. In the constant climate condition, the mean experimental elastic deflection of Group RC was 5.72 mm and the numerical model predicted a value of 5.76 mm. Thereafter, the numerical model closely matches the experimental creep deflection up to 75 weeks.

For Group RV, the measured elastic deflection of 5.44 mm compared well with the numerical prediction of 5.76 mm. Once the relative humidity was increased, the deflection increased rapidly. Experimentally, the initial increase in creep deflection was less in the reinforced than the unreinforced beams and this is also predicted numerically. With additional relative humidity cycles, the fluctuations in deflection have been successfully predicted; however, greater fluctuations in the predicted numerical deflections have been observed. After 75 weeks, the mean experimental Group RV deflection result of 10.10 mm has been accurately predicted by the numerical model with a simulated deflection result of 10.09 mm. It is noted that the peak deflection of each cycle matches the numerical model well, but the troughs are under predicted but the general trend of increasing deflection with repeated cycles has been accurately modelled.

The total measured and predicted mean longitudinal strains on the tension and compression faces of the reinforced beams are shown in Fig. 7. In the constant climate, the maximum tensile and compressive strains in the reinforced beams are significantly lower than in the unreinforced beams, demonstrating the beneficial effect of the reinforcement. For the reinforced Group RV, the

elastic tensile strain of 597 με predicted by the model is slightly higher than the mean experimental tensile strain of 577 με. On the compression face, the predicted elastic strain of −718 με is larger than the experimental result of −643 με. Although the elastic strain on the compression face is larger than that measured experimentally, the difference is not deemed significant.

A large increase in longitudinal strain during the first moisture content change can be seen. This irrecoverable mechano-sorptive component has been simulated accurately in the reinforced beam. The reduction in irrecoverable mechano-sorptive creep due to the reinforcement, observed experimentally, is also predicted by the numerical model. The fluctuations in strain with repeated cycles simulated using the numerical model match well on the tension face but are overpredicted on the compression face. After 75 weeks, the measured maximum compressive strain was −866 με while the model predicts a conservative value of −1068 με.

The reinforced beam model has adequately simulated the mean experimentally measured deflection and strain behaviour in a variable climate condition. The addition of the BFRP rod reinforcement into the model has been shown to simulate the beneficial reduction of vertical deflection in reinforced beams and has been shown to adequately predict the total longitudinal creep strain which comprises the viscoelastic, mechano-sorptive and the swelling/shrinkage strain, on both the tension and compression faces of the reinforced beams.

5. Summary and conclusion

Unreinforced and reinforced glued laminated beams have been subjected to long-term creep tests in a variable climate condition [51]. The experimental creep tests confirm that reinforcing timber with a material of superior properties has a positive effect on the mean deflection and longitudinal strain results in a variable climate. This reduction is currently not accounted for in the design of timber structures. A coupled hygro-mechanical finite element model has been developed to predict the behaviour of FRP reinforced timber elements when stressed under long-term load and simultaneously subjected to changes in relative humidity. The model incorporates elastic, viscoelastic, mechano-sorptive and swelling/shrinkage behaviour described using a UMAT user-
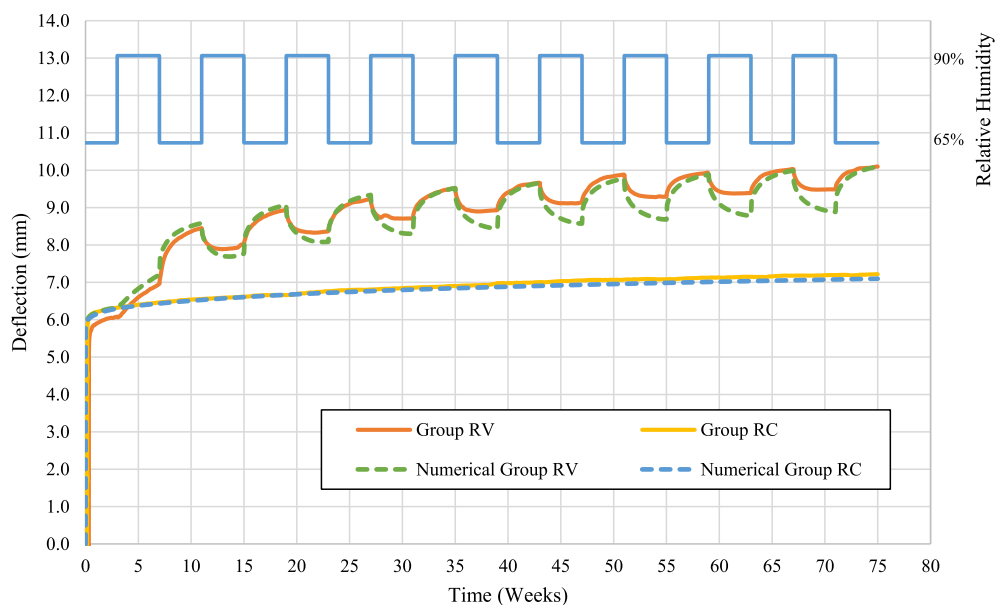
Fig. 6. Mean deflection result of Group RC (Constant climate) and Group RV (Variable climate) vs the numerical result.
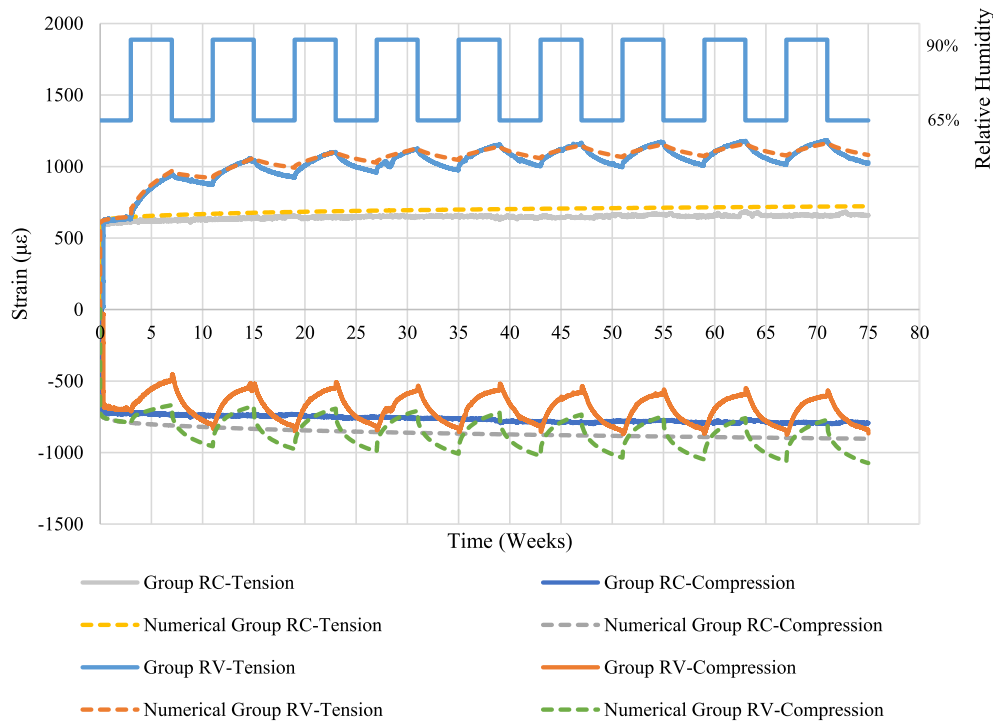
Fig. 7. Mean reinforced Group RC (Constant climate) and Group RV (Variable climate) experimental vs numerical longitudinal strain results.

subroutine in Abaqus finite elements software. Included in the formulation is an irrecoverable mechano-sorptive component. This irrecoverable component characterises the creep behaviour of stressed timber elements when the moisture content increases to a moisture content not previously attained. The climate conditions are implemented using a DFLUX subroutine and can be easily adapted to mimic other environmental conditions.

The following conclusions can be formulated based on the investigations presented on the long-term behaviour of FRP reinforced timber elements loaded in a constant or variable climate.

- The hygro-mechanical creep model has been shown to accurately predict the creep deflection of unreinforced and reinforced beams in both constant and variable climates. The model has also accurately predicted the reduced creep deflection behaviour of reinforced members in both constant and variable climates due to the addition of FRP reinforcement in the tension zone of the beams.
- The hygro-mechanical model has also accurately predicted the longitudinal creep strain measured on the tension and compression face of unreinforced and reinforced members. A beneficial reduction in longitudinal creep strain on the tension face of reinforced members, which was observed experimentally in both a constant and variable climate, has been simulated by the model.
- The irrecoverable mechano-sorptive creep matrix proposed by Fortino et al. [32] has been modified here to include the effects of irrecoverable creep in the longitudinal direction. This greatly improves the accuracy of the predictions of the long-term deflection and strain in both the unreinforced and reinforced beams in variable climates. It is recommended to include this modification in future studies, but it is noted that the parameters provided in this study have been calibrated against experimental test results on fast-grown Sitka spruce and should be checked when implemented on different species of timber.

- Long-term testing can be expensive and time-consuming. This validated hygro-mechanical model can now be used to examine other engineered wood products in different climates more quickly and at a significantly lower cost. In relation to reinforced elements, this model will be used in future parametric studies to investigate the influence of FRP type, percentage reinforcement area, and stress level on the creep behaviour of FRP reinforced beams with a view to determining creep modification factors for design.

CRediT authorship contribution statement

Conan O'Ceallaigh: Conceptualization, Data curation, Investigation, Methodology, Software, Writing - review & editing. **Karol Sikora:** Conceptualization, Writing - review & editing. **Daniel McPolin:** Funding acquisition, Supervision, Writing - review & editing. **Annette M. Harte:** Conceptualization, Funding acquisition, Supervision, Writing - review & editing.

Declaration of Competing Interest

The authors declare that they have no known competing financial interests or personal relationships that could have appeared to influence the work reported in this paper.

Acknowledgements

neering, NUI Galway, in particular, Peter Fahy, Colm Walsh and Gerard Hynes, is acknowledged.

References

[1] K.-U. Schober, A.M. Harte, R. Kliger, R. Jockwer, Q. Xu, J.-F. Chen, FRP reinforcement of timber structures, Constr. Build. Mater. 97 (2015) 106–118, https://doi.org/10.1016/j.conbuildmat.2015.06.020.

[2] I.R. Kliger, R. Haghani, M. Brunner, A.M. Harte, K.-U. Schober, Wood-based beams strengthened with FRP laminates: improved performance with pre-stressed systems, Eur. J. Wood Wood Prod. 74 (2016) 319–330, https://doi.org/10.1007/s00107-015-0970-5.

[3] S. Franke, B. Franke, A.M. Harte, Failure modes and reinforcement techniques for timber beams – State of the art, Constr. Build. Mater. 97 (2015) 2–13, https://doi.org/10.1016/j.conbuildmat.2015.06.021.

[4] J.R. Gilfillan, S.G. Gilbert, G.R.H. Patrick, The improved performance of home grown timber glulam beams using fibre reinforcement, J. Inst. Wood Sci. 15 (2001) 307–317.

[5] G. Raftery, A. Harte, Low-grade glued laminated timber reinforced with FRP plate, Compos. Part B Eng. 42 (2011) 724–735, https://doi.org/10.1016/j.compositesb.2011.01.029.

[6] E. McConnell, D. McPolin, S. Taylor, Post-tensioning of glulam timber with steel tendons, Constr. Build. Mater. 73 (2014) 426–433, https://doi.org/10.1016/j.conbuildmat.2014.09.079.

[7] A.M. Harte, P. Dietsch, Reinforcement of Timber Structures: A State-of-the-Art Report, Shaker Verlag GmbH, Germany, 2015.

[8] C. O'Neill, D. McPolin, S.E. Taylor, A.M. Harte, C. O'Ceallaigh, K.S. Sikora, Timber moment connections using glued-in basalt FRP rods, Constr. Build. Mater. 145 (2017) 226–235, https://doi.org/10.1016/j.conbuildmat.2017.03.241.

[9] H. Yang, W. Liu, W. Lu, S. Zhu, Q. Geng, Flexural behavior of FRP and steel reinforced glulam beams: experimental and theoretical evaluation, Constr. Build. Mater. 106 (2016) 550–563, https://doi.org/10.1016/j.conbuildmat.2015.12.135.

[10] W. Lu, Z. Ling, Q. Geng, W. Liu, H. Yang, K. Yue, Study on flexural behaviour of glulam beams reinforced by near surface mounted (NSM) CFRP laminates, Constr. Build. Mater. 91 (2015) 23–31, https://doi.org/10.1016/j.conbuildmat.2015.04.050.

[11] J. Senft, S. Suddarth, An analysis of creep-inducing stress in Sitka spruce, Wood Fiber Sci. 2 (1971) 321–327.

[12] T. Toratti, Creep of timber beams in a variable environment, Laboratory of Structural Engineering and Building Physics, Helsinki University of Technology, Finland, 1992.

[13] R.W. Davidson, The influence of temperature on creep in wood, For. Prod. J. 12 (1962) 377–381.

[14] S. Hering, P. Niemz, Moisture-dependent, viscoelastic creep of European beech wood in longitudinal direction, Eur. J. Wood Wood Prod. 70 (2012) 667–670, https://doi.org/10.1007/s00107-012-0600-4.

[15] N. Plevris, T. Triantafillou, Creep behavior of FRP-reinforced wood members, J. Struct. Eng. 121 (1995) 174–186, https://doi.org/10.1061/(ASCE)0733-9445(1995)121:2(174).

[16] M. Yahyaei-Moayyed, F. Taheri, Creep response of glued-laminated beam reinforced with pre-stressed sub-laminated composite, Constr. Build. Mater. 25 (2011) 2495–2506, https://doi.org/10.1016/j.conbuildmat.2010.11.078.

[17] C. O'Ceallaigh, K. Sikora, D. McPolin, A.M. Harte, An investigation of the viscoelastic creep behaviour of basalt fibre reinforced timber elements, Constr. Build. Mater. 187 (2018) 220–230, https://doi.org/10.1016/j.conbuildmat.2018.07.193.

[18] S. Hučč, S. Svensson, Coupled two-dimensional modeling of viscoelastic creep of wood, Wood Sci. A 52 (2018) 29–43, https://doi.org/10.1007/S00226-017-0944-3.

[19] J.C. Simo, T.J.R. Hughes, Computational Inelasticity, Springer-Verlag, New York, USA, 1998. doi:10.1016/S0898-1221(99)90413-3.

[20] P. Gressel, Prediction of long-term deformation behaviour from short-term creep experiments, Holz Als Roh-Und Werkst. 42 (1984) 293–301, https://doi.org/10.1007/BF02608938.

[21] R.H. Leicester, A rheological model for mechano-sorptive deflections of beams, Wood Sci. Technol. 5 (1971) 211–220, https://doi.org/10.1007/BF00353683.

[22] A. Ranta-Maunus, A study of the creep of plywood, Report 5. 85 p +app.7p, Espoo:Technical Research Centre of Finland (VTT). Strutural mechanics laboratory, 1976.

[23] T. Toratti, Modelling the creep of timber beams, J. Struct. Mech. 25 (1992) 12–15.

[24] S. Fortino, P. Hradil, A. Genoese, A. Genoese, A. Pousette, Numerical hygro-thermal analysis of coated wooden bridge members exposed to Northern European climates, Constr. Build. Mater. 208 (2019) 492–505, https://doi.org/10.1016/j.conbuildmat.2019.03.012.

[25] A. Mårtensson, Creep behaviour of structural timber under varying humidity conditions, J. Struct. Eng. 120 (1994).

[26] A. Ranta-Maunus, The viscoelasticity of wood at varying moisture content, Wood Sci. Technol. 9 (1975) 189–205, https://doi.org/10.1007/BF00364637.

[27] K. Fridley, R.C. Tang, L. Soltis, Creep behavior model for structural lumber, J. Struct. Eng. New York, N.Y. 118 (1992) 2261–2276.

[28] S. Mohager, T. Toratti, Long term bending creep of wood in cyclic relative humidity, Wood Sci. Technol. 27 (1992) 49–59, https://doi.org/10.1007/BF00203409.

[29] J. Lu, R. Leicester, Effect of cyclic humidity exposure on moisture diffusion in wood, Wood Fiber Sci. 29 (1997) 68–74.

[30] A. Hanhijärvi, P. Mackenzie-Helnwein, Computational analysis of quality reduction during drying of lumber due to irrecoverable deformation. I: orthotropic viscoelastic-mechanosorptive-plastic material model for the transverse plane of wood, J. Eng. Mech. 129 (2003) 996–1005, https://doi.org/10.1061/(ASCE)0733-9399(2003)129: 9(996).

[31] A. Hanhijärvi, Deformation properties of Finnish spruce and pine wood in tangential and radial directions in association to high temperature drying: Part IV. Modelling, Holz Als Roh - Und Werkst. 58 (2000) 211–216. doi:10.1007/s001070050415.

[32] S. Fortino, F. Mirianon, T. Toratti, A 3D moisture-stress FEM analysis for time dependent problems in timber structures, Mech. Time-Dependent Mater. 13 (2009) 333–356, https://doi.org/10.1007/s11043-009-9103-z.

[33] M. Leivo, On the stiffness changes in nail plate trusses VTT Technical Research Centre of Finland, 1991.

[34] T. Toratti, S. Svensson, Mechano-sorptive experiments perpendicular to grain under tensile and compressive loads, Wood Sci. Technol. 34 (2000) 317–326, https://doi.org/10.1007/s002260000059.

[35] S. Svensson, T. Toratti, Mechanical response of wood perpendicular to grain when subjected to changes of humidity, Wood Sci. Technol. 36 (2002) 145–156, https://doi.org/10.1007/s00226-001-0130-4.

[36] J. Jönsson, Moisture Induced Stresses in Timber Structures, Division of Structural Engineering, Lund University of Technology, Sweden, 2005.

[37] M. Fragiacomo, S. Fortino, D. Tononi, I. Usardi, T. Toratti, Moisture-induced stresses perpendicular to grain in cross-sections of timber members exposed to different climates, Eng. Struct. 33 (2011) 3071–3078.

[38] F.M. Massaro, K.A. Malo, Modelling the viscoelastic mechanosorptive behaviour of Norway spruce under long-term compression perpendicular to the grain, Holzforschung 73 (2019) 715–725.

[39] F.M. Massaro, K.A. Malo, Long - term behaviour of Norway spruce glulam loaded perpendicular to grain, Eur. J. Wood Wood Prod. (2019), https://doi.org/10.1007/s00107-019-01437-4.

[40] S. Hučč, S. Svensson, T. Hozjan, Hygro-mechanical analysis of wood subjected to constant mechanical load and varying relative humidity, Holzforschung 72 (2018) 863–870.

[41] D.A. Tingley, The Stress-Strain Relationships in Wood and Fiber-Reinforced Plastic Laminae of Reinforced Glued-Laminated Wood Beams, Oregon State University, USA, 1996.

[42] E. Serrano, Glued-in rods for timber structures—a 3D model and finite element parameter studies, Int. J. Adhes. Adhes. 21 (2001) 115–127.

[43] P. Alam, The Reinforcement of Timber for Structural Applications and Repair, University of Bath, 2004.

[44] G. Raftery, A. Harte, Nonlinear numerical modelling of FRP reinforced glued laminated timber, Compos. Part B-Eng. 52 (2013) 40–50, https://doi.org/10.1016/j.compositesb.2013.03.038.

[45] W.G. Davids, H.J. Dagher, J.M. Breton, Modeling creep deformations of FRP-reinforced glulam beams, Wood Fiber Sci. 32 (2000) 426–441.

[46] S. Fortino, P. Hradil, G. Metelli, Moisture-induced stresses in large glulam beams. Case study: vihantasalmi bridge, Wood Mater. Sci. Eng. 14 (2019) 366–380, https://doi.org/10.1080/17480272.2019.1638828.

[47] Abaqus, Abaqus Documentation Version 6.14-1, Dassault Systémes Simulia Corporation, Providence, RI, USA, 2014

[48] F. Mirianon, S. Fortino, T. Toratti, A method to model wood by using ABAQUS finite element software: Part 1. Constitutive Model and Computational Details, VTT Publication 687, VTT Technical Research Centre of Finland, 2008.

[49] K. Santaoja, T. Leino, A. Ranta-Maunus, A. Hanhijärvi, Mechanosorptive structural analysis of wood by the ABAQUS finite element program., Technical Research Centre of Finland, Research notes 1276, 1991

[50] A. Mårtensson, Mechano-sorptive effects in wooden material, Wood Sci. Technol. 28 (1994) 437–449, https://doi.org/10.1007/BF00225463.

[51] C. O'Ceallaigh, An Investigation of the Viscoelastic and Mechano-sorptive Creep Behaviour of Reinforced Timber Elements, PhD Thesis, National University of Ireland Galway, 2016.

[52] C. O'Ceallaigh, K. Sikora, D. McPolin, A.M. Harte, Viscoelastic Creep in Reinforced Glulam, in: Proc. 2016 World Conf. Timber Eng., Vienna, Austria, 2016.

[53] C. O'Ceallaigh, K. Sikora, D. McPolin, A.M. Harte, Mechano-sorptive Creep in Reinforced Glulam, in: Proc. WCTE 2018 World Conf. Timber Eng. Seoul, Rep. Korea, August 20-23, 2018

[54] C. O'Ceallaigh, K. Sikora, D. McPolin, A.M. Harte, The mechano-sorptive creep behaviour of basalt FRP reinforced timber elements in a variable climate, Eng. Struct. 200 (2019), https://doi.org/10.1016/j.engstruct.2019.109702 109702.

[55] CEN, EN 338. Structural timber - Strength classes, Comité Européen de Normalisation, Brussels, Belgium, 2016

[56] J. Bodig, B.A. Jayne, Mechanics of Wood Composites, Reprinted edition., Von Nostrand Reinhold Company, New York, Cincinnati, Toronto, 1993.

[57] P. Mackenzie-Helnwein, A. Hanhijärvi, Computational analysis of quality reduction during drying of lumber due to irrecoverable deformation. II: algorithmic aspects and practical application, J. Eng. Mech. 129 (2003) 1006–1016, https://doi.org/10.1061/(ASCE)0733-9399(2003)129: 9(1006).

[58] A. Hanhijärvi, Modelling of Creep Deformation Mechanisms in Wood, Technical Research Center of Finland Espoo, Finland, 1995.

[59] S. Ormarsson, Numerical analysis of Moisture-Related Distortions in Sawn Timber, PhD Thesis, Chalmers University of Technology, Gothenburg, Sweden, 1999.

[60] S. Ormarsson, O. Dahlblom, H. Petersson, A numerical study of the shape stability of sawn timber subjected to moisture variation Part 2: Simulation of drying board, Wood Sci. Technol. 33 (1999) 407–423, https://doi.org/10.1007/s002260050126.

[61] C. O'Ceallaigh, K. Sikora, D. McPolin, A.M. Harte, An experimental and numerical study of moisture transport and moisture-induced strain in fast-grown sitka spruce, Cienc. y Tecnol. 21 (2019) 45–64, https://doi.org/10.4067/S0718-221X2019005000105.

[62] D.G. Hunt, C.F. Shelton, Longitudinal moisture-shrinkage coefficients of softwood at the mechano-sorptive creep limit, Wood Sci. Technol. 22 (1988) 199–210, https://doi.org/10.1007/BF00386014.

[63] W. Davids, H. Dagher, J. Breton, Experimental and numerical study on creep of FRP reinforced glulam beams, in: L. Bostrom (Ed.), Proc. 1st RILEM Symp. Timber Eng. RILEM, Stockholm, Sweden, 13-15 September, 1999: pp. 581–590.

[64] G. Raftery, A. Harte, P. Rodd, Qualification of wood adhesives for structural softwood glulam with large juvenile wood content, J. Inst. Wood Sci. 18 (2008) 24–34.

[65] C. Zachary, S. Kavan, Feasibility of strengthening glulam beams with prestressed basalt fibre reinforced polymers, Masters Thesis, Department of Civil and Environmental Engineering, Division of Structural Engineering, Chalmers University of Technology, 2012.

[66] Rotafix, Material Data Sheet, Rotafix House, Abercraf, Swansea, SA9 1UR, U.K. Accesed www.rotafix.co.uk/ 29th April 2014, 2014.

[67] J. Konnerth, W. Gindl, U. Müller, Elastic properties of adhesive polymers. I. Polymer films by means of electronic speckle pattern interferometry, J. Appl. Polym. Sci. 103 (2007) 3936–3939, https://doi.org/10.1002/app.24434.

[68] D.G. Hunt, Limited mechano-sorptive creep of beech wood, J. Inst. Wood Sci. 9 (1982) 136–138.